AIMS Mathematics, 11(6): 18329–18360.
DOI: 10.3934/math.2026745
Received: 21 February 2026
Revised: 09 June 2026
Accepted: 15 June 2026
Published: 22 June 2026

http://www.aimspress.com/journal/Math

Research article

Lifetime prediction and reliability modeling of perovskite solar cells using the proportional Hazard Chen model

Hanan Haj Ahmad[1,*], Sameh Abdellatif[2], Yazan Rabaiah[3] and Mohamed Aboshady[4]

[1] Department of Mathematics and Statistics, College of Science, King Faisal University, Al-Ahsa 31982, Saudi Arabia
[2] The Electrical Engineering department and FabLab, at the Centre of Emerging Learning Technologies CELT, British University in Egypt (BUE), 11387, Cairo, Egypt
[3] Department of Electrical Engineering, College of Engineering, King Faisal University, Hofuf 31982, Al Ahsa, Saudi Arabia
[4] Department of Basic Science, Faculty of Engineering, British University in Egypt (BUE), 11387, Cairo, Egypt

* **Correspondence:** Email: hhajahmed@kfu.edu.sa; Tel: 00966542113743; Fax: 00966135897094.

Abstract: This study introduces a reliability-based framework that quantifies perovskite solar cell (PSC) degradation by estimating the T80 lifetime (time to 80% of initial power conversion efficiency) from experimental aging data using exponential regression. The resulting failure times, collected under an adaptive progressive Type-II censoring scheme, were analyzed using the Proportional Hazard Chen (PHC) distribution. This model accommodates increasing hazard rates characteristic of PSC aging mechanisms. Model parameters were estimated using maximum likelihood estimation (MLE) and Bayesian inference, enabling comprehensive reliability metrics including survival probability, hazard rate, and mean time to failure (MTTF). The procedure was validated using degradation data from PSCs with titanium dioxide and nickel oxide transport layers, supplemented by Solar Cell Capacitance Simulator (SCAPS). The empirical results show that the survival probability decreases from approximately 0.98 at 0.5 hours to below 0.02 at 17 hours, while the hazard rate increases from approximately 0.04 to above 0.75, confirming an accelerating degradation pattern. The Monte Carlo simulation study further demonstrates that both MLE and Bayesian approaches can estimate the PHC model effectively, with improved accuracy when the effective number of observed failures and the termination time increase. Bayesian inference provides more conservative long-term reliability and MTTF predictions under heavy censoring, making it useful for risk-aware lifetime assessment. Overall, the proposed framework provides a practical statistical tool for predicting, comparing, and benchmarking PSC lifetimes in photovoltaic reliability studies.

Keywords: perovskite solar cells; reliability analysis; proportional Hazard model; Bayesian inference;

progressive censoring; regression analysis
Mathematics Subject Classification: 62J02, 62F10, 62F15, 62N01, 62N05

Abbreviations

Abbrev.	Definition	Abbrev.	Definition
AIC	Akaike Information Criterion	MCMC	Markov Chain Monte Carlo
BIC	Bayesian Information Criterion	M-H	Metropolis-Hastings algorithm
CI	Confidence Interval	MLE	Maximum Likelihood Estimation
CRI	Credible Interval	MSE	Mean Squared Error
$CsPbX_3$	Cesium Lead Halide (X = I, Br, Cl)	MTTF	Mean Time To Failure
FTO	Fluorine-doped Tin Oxide	NiO	Nickel Oxide
HTL	Hole Transport Layer	PDF	Probability Density Function
IQR	Interquartile Range	PH	Proportional Hazard
KDE	Kernel Density Estimate	PHC	Proportional Hazard Chen
LED	Light-Emitting Diode	PSC	Perovskite Solar Cell
RMSE	Root-Mean-Square Error	SCAPS	Solar Cell Capacitance Simulator
SEL	Squared Error Loss	SMU	Source Measurement Unit
TiO_2	Titanium Dioxide		

1. Introduction

Perovskite solar cells represent a transformative step forward in photovoltaic technology; however, the market's success depends on mitigating critical stability issues. This section highlights the basic degradation mechanisms influencing PSCs and explains the need for complex reliability modeling strategies. We introduce a statistical framework that addresses these reliability concerns by employing advanced censoring schemes and flexible lifetime distributions.

1.1. PSC stability and lifetime metrics

Perovskite solar cells have emerged as a groundbreaking technology in the field of photovoltaics, characterized by their unique crystal structure and notable efficiency [1]. Named after the mineral perovskite, these solar cells typically consist of a hybrid organic-inorganic lead or tin halide-based material, which allows efficient light absorption and charge carrier generation [2–4]. Since their inception, PSCs have rapidly gained attention for their potential to achieve efficiencies that exceed 25%, competing with traditional silicon-based solar cells while offering lower production costs and simpler manufacturing processes [1]. A review of PSCs for space photovoltaics has been provided by [5], emphasizing their high power-to-weight potential and reported resilience to multiple radiation types, while stressing that long-term stability under vacuum and extreme thermal swings remains the main barrier. In [6], the reliability of PSCs was quantified by producing statistical descriptions of the response and estimating buckling risk/failure probabilities, enabling reliability-based safety assessment and design-oriented parametric studies. A reliability model of a wind-photovoltaic hybrid

power system and its complementary strategy and maintenance cost under different failure modes and scenarios has been studied by [7].

Despite their promising performance, the stability and longevity of PSCs remain significant challenges that impact their commercial viability [8–10]

In principle, the degradation over time in PSCs can be attributed to several factors:

- Environmental conditions can be considered as the main reported degradation factor for solar cells [10].
- Exposure to moisture, oxygen, and UV radiation can lead to the degradation of the perovskite material [11, 12].
- Humidity is particularly harmful, since it can break down the perovskite structure, resulting in decreased cell efficiency [4, 13].
- Perovskite materials can be sensitive to temperature variation. High temperatures can accelerate degradation processes, leading to phase changes and the formation of inactive units [4, 14].
- The movement of ions within the perovskite layer can cause the formation of defective cells, which can negatively affect the electrical properties of the solar cell. This ion migration can be exacerbated under operating conditions, particularly in the presence of an electric field [15–17].
- Prolonged exposure to sunlight can also contribute to the degradation of perovskite materials. Photodegradation can alter the optical and electronic properties of the material, ultimately reducing the efficiency of solar cells [3, 18].

1.2. Reliability modeling and censored data

Robust lifetime inference requires models that (i) accommodate non-monotone and protocol-dependent hazard shapes and (ii) extract reliable parameters from incomplete experiments, where practical constraints force early withdrawals or fixed failure counts. However, it is sometimes planned to terminate the experiment earlier to save the time and cost of the experimental units.

Accelerated aging of PSCs is costly in time and sample resources; devices are usually removed before failure (right-censoring), and experiments are commonly designed with a fixed number of observed failures (Type-II censoring). Progressive Type-II censoring enhances efficiency by enabling planned removals at successive failures, thereby concentrating information near the tail of interest; see [19]. The adaptive progressive Type-II scheme goes further: After each observed failure time, the next removal size can be chosen based on the data realized to that point (within a prespecified plan), balancing precision and experimental time/cost; see [20]. This adaptivity yields tighter inference for lifetime and reliability functions under the same resource budget, a natural fit for PSCs' stability campaigns where stress conditions and failure rates can evolve during testing.

PSCs can show early burn-in, midlife stabilization, or late-stage acceleration, calling for models beyond simple exponential or Weibull. The Chen distribution is a well-studied, two-parameter lifetime that admits increasing, decreasing, and bathtub-shaped hazards; modern extensions further enhance flexibility. Embedding Chen within a proportional hazard (PH) structure allows covariates or protocol indicators (light profile, temperature, encapsulation) to scale risk multiplicatively while retaining a tractable baseline.

For adaptive progressive Type-II samples, MLE provides efficient point estimates and asymptotic standard errors for model parameters and derived quantities and reliability at mission time. Bayesian

methods complement MLE by (a) stabilizing inference under heavy censoring via prior information and (b) delivering full posterior uncertainty for lifetimes and reliability curves when comparing device designs or qualifying thresholds. The likelihoods, information matrices, and computational strategies, such as Markov chain Monte Carlo (MCMC), are tailored to progressive adaptive schemes across many lifetime families, which directly transfer to proportional hazard Chen modeling.

Recent studies have highlighted the role of flexible lifetime distributions and advanced inference methods in reliability analysis under incomplete data. Hassan et al. [21] studied Burr XII reliability under extreme conditions using upper record values, while Hassan and Almetwally [22] investigated multi-stress-strength reliability for the inverse Weibull distribution under progressive Type-II censoring with random removal. The present work extends this direction by modeling PSC T80 lifetimes using the PHC distribution under adaptive progressive Type-II censoring with MLE and Bayesian estimation.

1.3. The PHC model

The Chen distribution, first introduced by Chen [23], is a flexible and versatile model widely used for analyzing time and reliability data. One of its key advantages lies in its ability to accommodate various shapes of the hazard function, including increasing, decreasing, and bathtub-shaped patterns, which are commonly observed in practical reliability scenarios. This makes it notably suitable for modeling failure times of high-reliability components, mechanical systems, and biological experiments.

Recently, the Chen distribution has gained significant attention due to its mathematical feasibility and adaptability to several censoring and truncation schemes. Its parameters offer natural control over the scale and shape of the distribution, allowing it to reflect complex aging behaviors and diversity in the data. These features make it a powerful choice for applications in industrial reliability testing, biomedical survival analysis, and engineering systems.

Let X be a random variable with the Chen distribution. The probability density function (PDF) and the survival function of X are defined as follows:

$$g(x;\alpha,\beta) = \alpha\beta x^{\beta-1} e^{x^{\beta}} e^{\alpha(1-e^{x^{\beta}})}, \tag{1.1}$$

$$\bar{G}(x;\alpha,\beta) = e^{\alpha(1-e^{x^{\beta}})}, \tag{1.2}$$

respectively, where the support $x \geq 0$, $\beta > 0$ is the shape parameter and $\alpha > 0$ is the scale parameter of the model. For further details and statistical properties about the Chen distribution, refer to Ahmed et al. [24].

This study involves the statistical inference of the unknown parameters of the proportional hazard Chen distribution, which is used to model and assess the time-dependent deterioration of perovskite solar cells. The proportional hazard Chen distribution, denoted by PHC, is a new version of the Chen distribution. The adaptability of the Chen distribution makes it suitable for studying time-dependent system failures and the availability of events in diverse applications, such as solar cell efficiency and other mechanical system reliability.

Unlike the basic Chen model, the PHC model extends the analysis by including the covariates (X_i), such that the hazard function of PHC is written as:

$$h(x) = \gamma h_0(x),$$

where $h_0(x)$ is the hazard rate of the Chen distribution. This enables the interaction between external factors that determine system performance, such as environmental issues. Additionally, it improves decision-making by providing a quantitative assessment of how specific variables contribute to the overall system reliability and longevity.

Applying the idea of proportional hazard transform on the Chen distribution, which is obtained using the following transformation:

$$\bar{F}(x;\gamma) = [\bar{G}(x)]^{\gamma},$$

where $\bar{F}$ is the survival function of the new PHC model denoted by $S(x)$. For more details on the proportional hazard model, refer to Kundu [25]. This newly generated distribution has three parameters and is more flexible than the original Chen distribution. The PDF and the survival function for the PHC distribution are given, respectively, by

$$f(x;\alpha,\beta,\gamma) = \alpha\beta\gamma x^{\beta-1} exp[\alpha\gamma(1-e^{x^{\beta}}) + x^{\beta}], \tag{1.3}$$

$$\bar{F}(x;\alpha,\beta,\gamma) = exp[\alpha\gamma(1-e^{x^{\beta}})]. \tag{1.4}$$

The hazard rate function for the PHC distribution is given by

$$h(x) = \alpha\beta\gamma x^{\beta-1} e^{x^{\beta}}. \tag{1.5}$$

Figure 1 illustrates the plots for the PHC distribution, showing the PDF and the hazard rate function across parameter values that cover the main trends:

- $\beta \in (0,1)$: U-shaped hazard (diverges at 0, then decreases, then increases).
- $\beta = 1$: purely increasing (exponential-like) hazard.
- $\beta > 1$: starts at 0 and increases (convex).

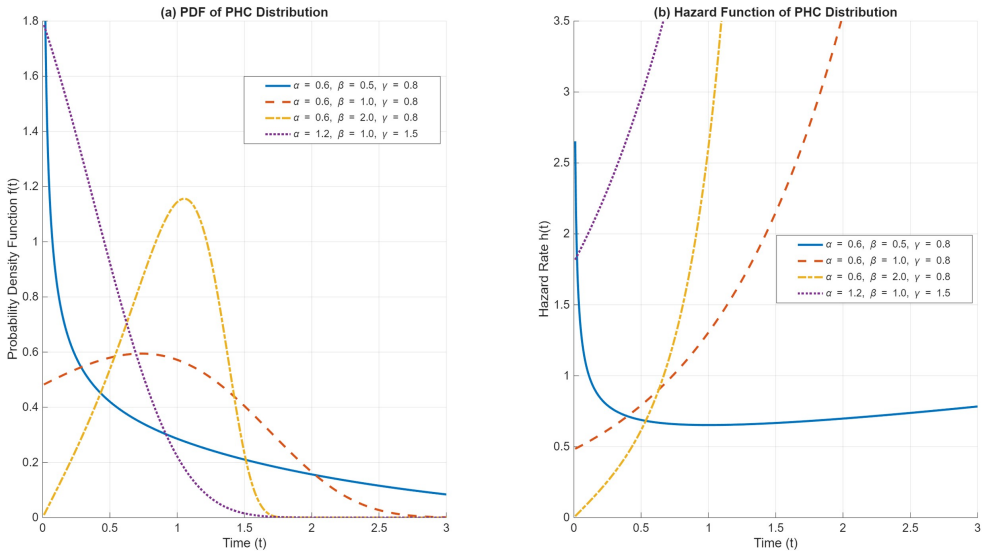

Figure 1. PDF and hazard rate plots for the PHC distribution.

The MTTF is obtained from the survival function as

$$\text{MTTF} = E(X) = \int_0^{\infty} S(t;\alpha,\beta,\gamma)\, dt. \tag{1.6}$$

Since this integral does not generally have a simple closed-form expression, it is evaluated numerically.

The PHC distribution was selected because it provides a flexible and interpretable framework for modeling PSC degradation data with time-dependent failure risk. Compared with the exponential distribution, which assumes a constant hazard rate, the PHC model can capture aging behavior through an increasing hazard function. Compared with the Weibull distribution, the PHC model offers additional flexibility through the Chen baseline and the proportional hazard parameter, making it suitable for censored reliability data where both the shape and level of the hazard are important. Lognormal and gamma distributions may be useful for skewed lifetime data, but their hazard functions are not always as directly aligned with proportional hazard reliability interpretation. Therefore, PHC is particularly useful when degradation risk increases with operating time and when survival probability, hazard rate, and MTTF are required under censored experimental designs.

1.4. Objectives and motivation

In recent years, the rapid advancement of PSC technology has led to significant improvements in efficiency and performance; however, there remains a notable gap in the mathematical modeling of their lifetime prediction and reliability assessment. While various approaches have been developed to analyze the degradation mechanisms of traditional solar cells, the unique properties and instability of perovskite materials necessitate tailored models that accurately capture their specific degradation behaviors under operational conditions. Current literature often lacks comprehensive frameworks that integrate advanced statistical methods, such as the Proportional Hazard Chen model, to effectively address the complexities of PSC degradation over time. Moreover, existing models frequently overlook critical factors such as adaptive progressive Type-II censoring, which can enhance the robustness of lifetime predictions. As such, there is a pressing need for innovative mathematical approaches that not only improve the accuracy of lifetime estimates for PSC but also facilitate their qualification for commercial applications, thereby bridging the gap between laboratory research and real-world deployment.

The main contribution of this work is the development of a unified reliability framework that converts PSC degradation curves into T80 lifetime data and analyzes these lifetimes using the PHC distribution under adaptive progressive Type-II censoring. This provides a statistically rigorous approach for estimating survival probability, hazard rate, and MTTF while accounting for incomplete lifetime observations.

We adopt the above framework to PSCs stability; hence, the degradation curves from controlled aging are preprocessed to estimate critical lifetime by regression analysis. Lifetime data are then modeled with a PHC distribution assuming adaptive progressive Type-II censoring samples; parameters are estimated by MLE and Bayesian inference to deliver rigorous lifetime and reliability predictions suitable for technology qualification and commercialization.

2. Materials and experimental methods

The experimental foundation of this study encompasses both the fabrication and the characterization of PSCs under controlled conditions. We specify the comprehensive methodology for device manufacturing, performance monitoring, and data gathering that generates the degradation dataset.

This systematic approach reinforces reproducible results that are essential for realistic reliability analysis and model validation.

2.1. Device fabrication and characterization

The cell investigated in this paper is the cesium lead halide ($CsPbX_3$, where X stands for halides such as iodine, bromine, or chlorine). To achieve optimal performance, the fabrication recipe involves a number of stack structure depositions. First, we prepare glass substrates coated with fluorine-doped tin oxide (FTO). The FTO substrate is then spin-coated with a thin layer of titanium dioxide (TiO_2); this electron transport layer (ETL), which has a high electron mobility, makes it easier to remove electrons from the active layer. The cesium lead halide layer is created by dissolving cesium lead ($CsPbI_3$) in isopropanol as a solvent and spin-coating it after annealing TiO_2. Similar methods are used to produce nickel oxide (NiO) as the hole transport layer (HTL), which is then annealed to improve its hole-conductive characteristics and enable efficient hole transport to the electrode while reducing recombination losses. Lastly, the full device structure is formed by attaching a second FTO layer as the counter electrode. A comprehensive recipe may be found in [3, 16, 26] and Figure 2.

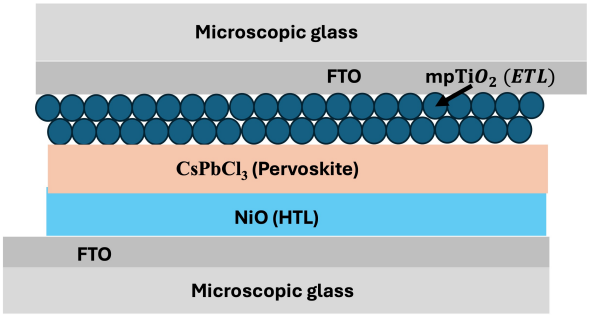

Figure 2. A schematic plot of a perovskite solar cell formation.

As the target of this study is to investigate the time-degradation behavior in PSCs, it is critical to track cell performance electrically. The manufactured PSCs are electrically characterized for this purpose. To excite the solar cells, we used our specially designed solar simulator with light-emitting diode (LED)-based 1-sun optical injection. As a class-C calibrated simulator, this configuration offers consistent illumination that closely resembles typical sun circumstances. Our Keithley Source Measurement Unit (SMU, 2410 series) is used to perform the measurements. The SMU supplies a systematic sweep of the voltage and measures the corresponding current, resulting in the current-voltage characteristics of the cell.

To enlarge our dataset, simulations are conducted using the SCAPS. This method allows modeling the optoelectronic characteristics of the solar cells by simulating carrier transport, recombination, and other phenomena. Through SCAPS, various input parameters, including but not limited to layer thickness, doping concentrations, and material properties, can be manipulated to identify optimal configurations that maximize solar cell efficiency. A detailed model is demonstrated in [15–17].

2.2. Data acquisition

The time-degradation behavior monitoring, associated with data acquisition for our fabricated PSC, is conducted using the Keithley SMU with the aid of LabView NXG, which collects data at regular

intervals of every 12 hours. Consequently, we experimentally tracked the solar cells' performance against time due to any environmental factors or material degradation. Additionally, to boost the experimental data, a simulation model was applied to assess potential cell degradation under varying conditions. This model considers factors such as temperature fluctuations, humidity, and light exposure as a variation in the material's effective parameters to model the long-term stability and efficiency of the solar cells; see [3, 15]. The combined data from the SMU and the simulation model provides a comprehensive dataset for the degradation mechanisms affecting solar cells.

In the context of PSC degradation, understanding the survival and hazard functions is crucial for engineering reliability. The survival function represents the probability that a PSC will maintain its performance above a certain threshold over time, which is commonly noted by the T_{80}, while the hazard function quantifies the instantaneous risk of failure at a specific time point (which is out of the scope of the current study and can be part of future work). By analyzing these functions, we can gain insights into the degradation behavior of PSCs under various environmental conditions, which is essential for predicting their operational lifespan. This analysis allows for the identification of critical degradation thresholds and the timing of potential failures, enabling engineers to make informed decisions regarding material selection, design modifications, and maintenance strategies. Ultimately, incorporating survival and hazard functions into our degradation monitoring framework enhances our understanding of PSC reliability, facilitating the development of more robust solar technologies that can withstand real-world operational challenges.

3. Degradation data modeling

This section implements the pre-filtering for the raw data that represents efficiency over different time spans, to extract the 80% predicted degradation times for solar cells.

3.1. Data preprocessing and normalization

To accurately determine the onset of performance decline, we conducted a thorough analysis of the initial efficiency metrics. This involves employing regression analysis, adjusting reference points, and designating "time zero" at day 5.5 of the experimental timeline. This specific choice of time zero is justified by the observed stability of the solar cells during the initial 5.5 days, wherein they exhibited minimal deviation in performance. Consequently, we excluded all data collected before this point, thereby establishing a robust baseline for our analysis. All samples were subsequently compared within this framework to ensure consistency throughout the evaluation period, utilizing MATLAB software for comprehensive data processing and analysis.

3.2. Stretched exponential regression modeling

We used nonlinear regression with an extended exponential function to simulate the decrease in efficiency of PSCs over time:

$$E(t) = A \cdot \exp\left(-(B \cdot t)^{\beta}\right), \tag{3.1}$$

where $E(t)$ represents the efficiency at time t. In materials science and photovoltaics, dispersive kinetics, heterogeneous degradation, and stretched relaxation processes are all described by the stretched exponential model [27]. This function permits non-exponential behavior that can capture

early rapid decline followed by a slower tail, in contrast to a simple exponential decay ($\beta = 1$). Because of its adaptability, it is especially well-suited for PSCs, where ion migration, interfacial recombination, and environmental conditions frequently cause efficiency loss to display intricate and multi-stage patterns. The degradation trajectory is determined by the following three parameters:

- A: Initial efficiency (scale parameter). Ideally $A \approx 1$ after normalization; deviations show measurement offset or early transient effects.
- B: Rate constant (inverse time scale). Faster overall degradation is implied by larger B.
- β: Stretch exponent. When $\beta < 1$, the degradation rate decreases over time (sub-exponential); when $\beta > 1$, the rate accelerates (super-exponential); $\beta = 1$ recovers the simple exponential decay. In our dataset, we consistently estimated $\beta < 1$, indicating sub-exponential degradation behavior.

Initially, we selected a random row of efficiency-time data. We divided the efficiency values by their initial values to standardize them and simplify the analysis. To obtain starting guesses for nonlinear fitting, we linearize the model. Taking logarithms twice gives

$$\log\left(-\log\left(\frac{E(t)}{A}\right)\right) = \beta \log B + \beta \log t. \tag{3.2}$$

We use a MATLAB code (see Appendix A) to construct a straightforward linear regression of $\log(-\log(E/A))$ against $\log t$ using the experimental $E(t)$ and an initial estimate of A (taken as the first measured efficiency at $t = 0$). An initial β is obtained from the regression's slope, while an initial $\log B$ is obtained from the intercept. The next nonlinear least-squares procedure uses these values as initial predictions.

The root-mean-square error (RMSE), $\mathrm{RMSE}(\hat{\theta}) = \sqrt{\frac{1}{N}\sum_{i=1}^{N}(\hat{\theta}_i - \theta)^2}$, and the modified R^2 coefficient are used to evaluate the goodness-of-fit. The same procedure is applied independently to each cell, as illustrated for the sample rows presented in Figure 3.

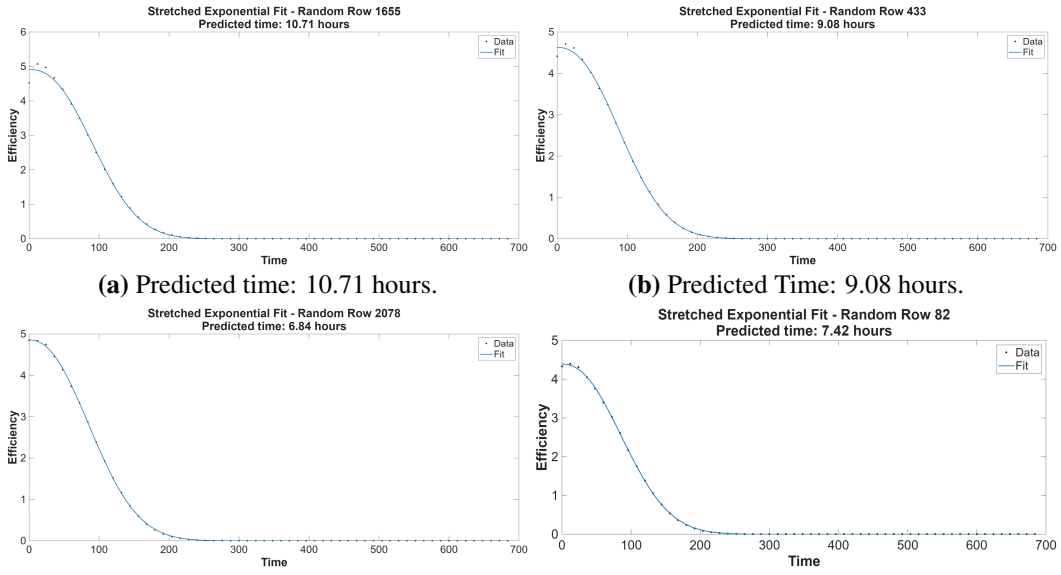

(a) Predicted time: 10.71 hours. **(b)** Predicted Time: 9.08 hours.

(c) Predicted Time: 6.84 hours. **(d)** Predicted Time: 7.42 hours.

Figure 3. Stretched exponential fit for four randomly selected solar cells.

We forecast the time at which efficiency decreases to 20% of its initial value (i.e., 80% degradation, designated T80) using the fitted model. After the 5.5-day mark, this estimated time is transformed into hours for simpler interpretation and further reliability analysis.

3.3. Predicted degradation times

To thoroughly examine the distribution and patterns of the predicted T80 values, Figure 4 presents four complementary statistical visualizations. Each subplot provides a distinct perspective on the underlying data structure, and together they offer a comprehensive characterization of the degradation time distribution.

- Top-left: Kernel Density Estimate (KDE): The kernel density estimate provides a smooth, continuous approximation of the probability density function of the predicted T80 times. Unlike a histogram, which depends on arbitrary bin choices, the KDE places a smooth kernel function (typically Gaussian) at each data point and sums these contributions. The resulting curve reveals the overall shape of the distribution, including modality (number of peaks), skewness (asymmetry), and tail behavior. In our data, the KDE shows a unimodal distribution with a slight rightward skew, indicating that most cells degrade within a central time window, with a minority taking longer to reach 80% degradation.
- Top-right: Histogram: The histogram groups the predicted T80 times into discrete bins (intervals) and displays the frequency (or count) of observations within each bin as vertical bars. This provides an intuitive, nonparametric view of the data distribution. The bin width was selected using Scott's rule to balance bias and variance. The histogram confirms the KDE's unimodal shape and reveals that the modal class (i.e., the most frequent degradation time) lies between approximately 8 and 10 hours. The histogram also makes it clear that very few cells degrade extremely quickly (below 4 hours) or survive beyond 16 hours.
- Bottom-left: Scatterplot: The scatterplot displays each individual predicted T80 time on the vertical axis against its observation index (order in the dataset) on the horizontal axis. This visualization is essential for detecting patterns that density estimates may obscure, such as:
  - Trends over time: A systematic upward or downward drift would indicate that later measurements differ from earlier ones (e.g., due to equipment drift or environmental changes). Our scatterplot shows no such trend, confirming stationarity.
  - Clustering: Distinct horizontal bands would suggest discrete subpopulations (e.g., cells from different fabrication batches). No clear clustering is observed.
  - Outliers: Isolated points far from the main cloud are easily identified. One potential outlier near 16 hours is visible but remains within plausible physical bounds.

  The random homogeneous dispersion of points supports the assumption that the T80 times are independent and identically distributed.
- Bottom-right: Boxplot: The boxplot (also known as box-and-whisker plot) provides a compact summary of five key percentiles: lower whisker, lower box edge (Q1), red line (median, Q2), upper box edge (Q3), upper whisker, and red crosses. The boxplot reveals that the median T80 is approximately 9.5 hours, the interquartile range (IQR = Q3 − Q1) spans from approximately 7.5 to 11.5 hours (indicating moderate spread), and the right whisker is longer than the left, confirming the right-skewed nature suggested by the KDE and histogram. No extreme outliers

beyond $3 \times$ IQR are present.

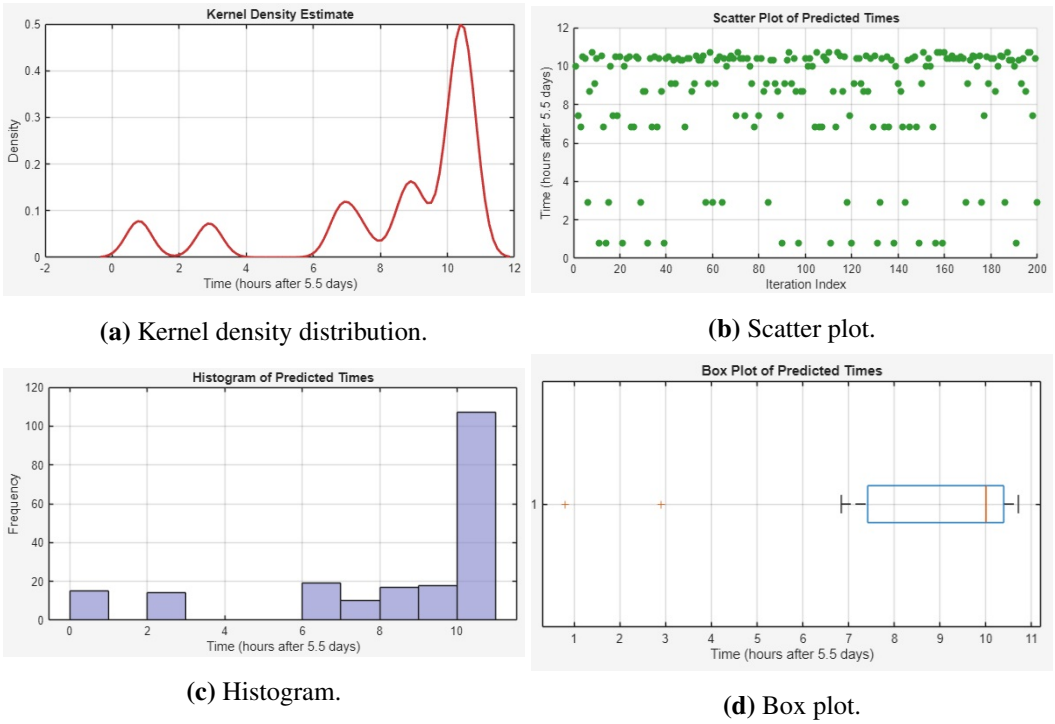

(a) Kernel density distribution.

(b) Scatter plot.

(c) Histogram.

(d) Box plot.

Figure 4. Distribution trends of predicted times for 20% efficiency.

Taken together, these four visualizations characterize the T80 degradation times as follows: unimodal, moderately right-skewed, centered around 9–10 hours, with no temporal trends or clustering, and minimal outliers. This distributional profile justifies the use of flexible lifetime models (such as the PHC distribution) that can accommodate positive skewness and moderate dispersion, while ruling out simple symmetric distributions (e.g., normal) that would be inappropriate for these data.

4. Statistical framework and theory

This section presents the mathematical framework for the analysis of censored lifetime data under adaptive progressive Type-II censoring schemes. We present the theoretical framework of the Proportional Hazard Chen distribution. The developed statistical machinery enables efficient parameter estimation while accommodating practical experimental constraints common in solar cell testing.

The adaptive Type-II progressive censoring scheme is a mixture of Type-I and Type-II progressive censoring, designed to address a key drawback of existing methods: the possibility of an undesirably small number of failures [20]. Traditional Type-I and hybrid censoring schemes can result in a very small (or even zero) effective sample size (m), making statistical inference inefficient or impossible. The proposed adaptive scheme guarantees that the effective sample size is always the pre-fixed number m. It does this by dynamically adjusting the number of items removed (R_i) during the experiment if it runs longer than a prespecified ideal time T, making it a superior and more practical choice for applications in reliability testing and survival analysis, where both time efficiency and data quality are paramount; see an example in [28]. The adaptive scheme works as follows:

- An integer $m < n$ and a progressive censoring plan $(R_1, R_2, ..., R_m)$ are pre-fixed.
- The experiment is run, removing R_i items after the i-th failure.
- If the m-th failure occurs before time T, the experiment is concluded normally.
- If time T is reached but only J failures have occurred (where $J < m$), the removal scheme is adapted for all subsequent failures: $R_{J+1} = ... = R_{m-1} = 0$. No more items are removed until the final (m-th) failure, at which point all remaining surviving units ($R_m = n - m - \sum_{i=1}^{J} R_i$) are removed. This strategy minimizes the total test time after T by keeping as many units under test as possible to hasten the remaining failures.

Figure 5 illustrates the evolution of the number of units on test under the adaptive Type-II progressive censoring scheme using a concrete example. We begin with $n = 20$ units and target $m = 8$ failures, with an ideal cutoff time $T = 100$. Before T, a pre-fixed removal plan $(R_1, \ldots, R_8) = (3, 2, 2, 1, 1, 2, 2, 2)$ applies, so each failure reduces the cohort by $1 + R_i$. The assumed failure times are $(10, 25, 40, 60, 95, 120, 145, 170)$. Because the fifth failure occurs at $t = 95 < T$, we have $J = 5$ failures before T. Once T is reached with only $J < m$, the scheme adapts by setting $R_{J+1} = \cdots = R_{m-1} = 0$; consequently, Failures 6 and 7 remove only the failed unit (drops of 1 each). At the m-th (eighth) failure, all remaining survivors are removed at once:

$$R_8 = n - m - \sum_{i=1}^{J} R_i = 20 - 8 - (3 + 2 + 2 + 1 + 1) = 3,$$

so the final drop is $1 + R_8 = 4$. Thus, the unshaded segment of the plot (before T) shows larger step decreases of size $1 + R_i$ under the planned scheme, whereas the shaded region (after T) shows the adaptive phase with minimal removals until the terminal failure, where the remaining cohort is cleared. This guarantees exactly m observed failures while minimizing additional test time after T.

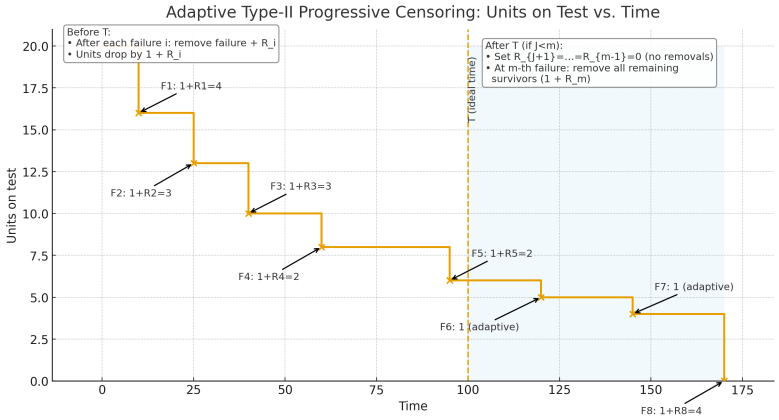

Figure 5. Adaptive progressive censoring scheme with n=20, m=8, T=100.

The adaptive progressive censoring scheme offers several practical benefits for PSC reliability testing. First, it avoids expensive test restarts by guaranteeing a fixed number of reported failures (m) even when deterioration goes more slowly than expected. Second, by guaranteeing that the experiment ends within a predetermined maximum period, it respects facility time limits. Third, to accelerate late-stage failures and provide fuller information on the lifespan distribution tail, which is crucial for long-term reliability prediction, more units are tested by setting ($R_i = 0$) during the adaptive

phase. Lastly, without affecting the lifetime study's statistical validity, the pre-planned removal strategy enables researchers to reuse undegraded cells for further analysis. Because of these characteristics, the adaptive progressive censoring method is especially well-suited for PSC aging campaigns with low resources.

5. Parameter estimation methodology

The main foundation of the reliability analysis is parameter estimation utilizing both Bayesian and iterative techniques. Using the MCMC reasoning, we develop maximum likelihood estimators with appropriate uncertainty values and complement them with Bayesian inference. When combined, these two methods solve the problems caused by controlled data and validate the overall parameter estimation.

5.1. Maximum likelihood estimation and confidence intervals

Let $x_{1:m:n} < x_{2:m:n} < \cdots < x_{m:m:n}$ denote the observed ordered failure times from an adaptive progressive Type-II censored sample, and let $\boldsymbol{\theta} = (\alpha, \beta, \gamma)$ be the vector parameter. The likelihood function under the adaptive progressive censoring scheme is given by

$$L(\boldsymbol{\theta}) = d_j \left[\prod_{i=1}^{m} f(x_{i:m:n}; \boldsymbol{\theta})\right] \left\{\prod_{i=1}^{j} [\bar{F}(x_{i:m:n}; \boldsymbol{\theta})]^{R_i}\right\} [\bar{F}(x_{m:m:n}; \boldsymbol{\theta})]^{\left(n-m-\sum_{i=1}^{j} R_i\right)}, \tag{5.1}$$

where d_j is defined as

$$d_j = \prod_{i=1}^{m} \left[n - i + 1 - \sum_{k=1}^{\max\{i-1, j\}} R_k\right].$$

Assume a random variable $X \sim \text{PHC}(\boldsymbol{\theta})$, then by substituting the PDF and the survival function given in Eqs (1.3) and (1.4), the likelihood follows:

$$\begin{aligned} L(\alpha, \beta, \gamma) = d_j &\left[\prod_{i=1}^{m} \alpha\beta\gamma x_{i:m:n}^{\beta-1} e^{x_{i:m:n}^{\beta}} e^{\alpha\gamma(1-e^{x_{i:m:n}^{\beta}})}\right] \\ &\times \left\{\prod_{i=1}^{j} \left[\exp\left(-\alpha\gamma\left[e^{x_{i:m:n}^{\beta}} - 1\right]\right)\right]^{R_i}\right\} \left[\exp\left(-\alpha\gamma\left[e^{x_{m:m:n}^{\beta}} - 1\right]\right)\right]^{n-m-\sum_{i=1}^{j} R_i}. \end{aligned} \tag{5.2}$$

Simplifying the above formula:

$$L(\alpha, \beta, \gamma) = d_j (\alpha\beta\gamma)^m \left(\prod_{i=1}^{m} x_i^{\beta-1} e^{x_i^{\beta}}\right) \exp\left(\alpha\gamma\left[n - T(\beta)\right]\right), \tag{5.3}$$

where

$$T(\beta) = \sum_{i=1}^{m} e^{x_i^{\beta}} + \sum_{i=1}^{j} R_i e^{x_i^{\beta}} + (n - m - \sum_{i=1}^{j} R_i) e^{x_m^{\beta}}.$$

The corresponding log-likelihood is

$$\ell(\alpha, \beta, \gamma) = \log d_j + m \log \alpha\gamma + m \log \beta + (\beta - 1) \sum_{i=1}^{m} \log x_i + \sum_{i=1}^{m} x_i^{\beta} + \alpha\gamma\left[n - T(\beta)\right]. \tag{5.4}$$

Solving the likelihood equations requires careful interpretation. From $\partial\ell/\partial\alpha = 0$ and $\partial\ell/\partial\gamma = 0$, we obtain

$$\frac{\partial\ell}{\partial\alpha} = \frac{m}{\alpha} + \gamma[n - T(\beta)] = 0 \quad \Rightarrow \quad \alpha = \frac{m}{\gamma[T(\beta) - n]}, \tag{5.5}$$

and

$$\frac{\partial\ell}{\partial\gamma} = \frac{m}{\gamma} + \alpha[n - T(\beta)] = 0 \quad \Rightarrow \quad \gamma = \frac{m}{\alpha[T(\beta) - n]}. \tag{5.6}$$

These are not closed-form solutions, because α depends on γ and β, and γ depends on α and β. Instead, they are profile likelihood expressions. Substituting either into the other gives $\alpha\gamma = m/[T(\beta) - n]$, which eliminates the individual dependence. The score equation for β is then reduced to a single nonlinear equation:

$$\frac{\partial\ell}{\partial\beta} = \frac{m}{\beta} + \sum_{i=1}^{m} \log x_i + \sum_{i=1}^{m} x_i^{\beta} \log x_i - \frac{m\,T'(\beta)}{T(\beta) - n} = 0, \tag{5.7}$$

where we have used $\alpha\gamma = m/[T(\beta) - n]$, and

$$T'(\beta) = \sum_{i=1}^{m} e^{x_i^{\beta}} x_i^{\beta} \log x_i + \sum_{i=1}^{j} R_i e^{x_i^{\beta}} x_i^{\beta} \log x_i + \left(n - m - \sum_{i=1}^{j} R_i\right) e^{x_m^{\beta}} x_m^{\beta} \log x_m.$$

This equation is solved numerically for $\hat{\beta}$ using the Newton-Raphson method. Once $\hat{\beta}$ is obtained, $\hat{\alpha}$ and $\hat{\gamma}$ are computed from $\hat{\alpha}\hat{\gamma} = m/[T(\hat{\beta}) - n]$, with individual values determined up to a scaling factor that is resolved by the original score equations.

Under standard regularity conditions, the maximum likelihood estimators (MLEs) $\hat{\boldsymbol{\theta}} = (\hat{\alpha}, \hat{\beta}, \hat{\gamma})$ are consistent and asymptotically normally distributed with the mean equal to the true parameter vector $\boldsymbol{\theta} = (\alpha, \beta, \gamma)$.

The final estimates are then substituted into the observed Fisher information matrix to obtain the asymptotic standard errors and the corresponding Wald confidence intervals.

5.1.1. Observed Fisher (negative Hessian) matrix

Let $H(\boldsymbol{\theta})$ denote the Hessian matrix with entries $\partial^2\ell/\partial a\,\partial b$, $a, b \in \{\alpha, \beta, \gamma\}$. The second derivatives are given by

$$\frac{\partial^2\ell}{\partial\alpha^2} = -\frac{m}{\alpha^2}, \qquad \frac{\partial^2\ell}{\partial\gamma^2} = -\frac{m}{\gamma^2}, \qquad \frac{\partial^2\ell}{\partial\alpha\,\partial\gamma} = \frac{\partial^2\ell}{\partial\gamma\,\partial\alpha} = n - T(\beta),$$

$$\frac{\partial^2\ell}{\partial\alpha\,\partial\beta} = \frac{\partial}{\partial\beta}\left[\frac{m}{\alpha} + \gamma\{n - T(\beta)\}\right] = -\gamma\,T'(\beta), \qquad \frac{\partial^2\ell}{\partial\gamma\,\partial\beta} = -\alpha\,T'(\beta),$$

$$\frac{\partial^2\ell}{\partial\beta^2} = -\frac{m}{\beta^2} + \sum_{i=1}^{m} x_i^{\beta}(\log x_i)^2 - \alpha\gamma\,T''(\beta),$$

where $T''(\beta)$ is obtained by differentiating $T'(\beta)$ as

$$T''(\beta) = \sum_{i=1}^{m} e^{x_i^{\beta}} x_i^{\beta}(\log x_i)^2 \left(x_i^{\beta} + 1\right) + \sum_{i=1}^{j} R_i e^{x_i^{\beta}} x_i^{\beta}(\log x_i)^2 \left(x_i^{\beta} + 1\right) + \left(n - m - \sum_{i=1}^{j} R_i\right) e^{x_m^{\beta}} x_m^{\beta}(\log x_m)^2 \left(x_m^{\beta} + 1\right).$$

The observed Fisher information matrix is defined as the negative Hessian matrix,

$$J(\theta) = -H(\theta).$$

Therefore,

$$J(\theta) = \begin{pmatrix} \frac{m}{\alpha^2} & \gamma T'(\beta) & T(\beta) - n \\ \gamma T'(\beta) & \frac{m}{\beta^2} - \sum_{i=1}^{m} x_i^{\beta} (\log x_i)^2 + \alpha\gamma T''(\beta) & \alpha T'(\beta) \\ T(\beta) - n & \alpha T'(\beta) & \frac{m}{\gamma^2} \end{pmatrix}.$$

5.1.2. Asymptotic covariance and Wald intervals

Let $\widehat{\boldsymbol{\theta}} = (\widehat{\alpha}, \widehat{\beta}, \widehat{\gamma})$ be the MLE. The large-sample covariance matrix can be estimated by the inverse observed information,

$$\widehat{\mathrm{Var}}(\widehat{\boldsymbol{\theta}}) \;=\; J(\widehat{\boldsymbol{\theta}})^{-1}.$$

The approximate standard errors are the square roots of the diagonal elements of $J(\widehat{\boldsymbol{\theta}})^{-1}$.

For a scalar component $\theta_k \in \{\alpha, \beta, \gamma\}$, a $(1-\eta) \times 100\%$ Wald confidence interval is

$$\widehat{\theta}_k \;\pm\; z_{1-\eta/2} \;\sqrt{\left[J(\widehat{\boldsymbol{\theta}})^{-1}\right]_{kk}}\,. \tag{5.8}$$

5.2. Bayesian estimation with MCMC

Under adaptive progressive censoring, particularly with small m or heavy censoring, maximum likelihood estimation can yield unstable estimates for parameters governing tail behavior (α, γ). Bayesian inference addresses this by (i) regularizing estimation through prior information, (ii) providing full posterior distributions rather than point estimates with asymptotic approximations, and (iii) delivering coherent uncertainty quantification for long-term reliability predictions (e.g., survival probabilities at late times). When prior information is limited, a practical Bayesian approach involves selecting a prior distribution that ensures analytical tractability in the updating process from prior to posterior. The available, although limited, prior knowledge is then utilized to determine the hyperparameters of this distribution, thereby maintaining both computational simplicity and coherence with the underlying uncertainty structure.

It is generally advisable to select a prior distribution that is not overly concentrated around any specific value; that is, a distribution characterized by a large variance. Under such circumstances, most of the inferential information will be contributed by the data, and the resulting posterior distribution will be primarily data-driven, i.e., $f(x \mid data) \approx f(x)$. To reflect vague or weak prior knowledge, it is common practice to adopt a conjugate prior corresponding to the assumed model for x, chosen to be as diffuse as possible so that it imposes minimal influence on the posterior inference while preserving analytical convenience. In Bayesian inference, Jeffreys' prior provides an objective and non-informative approach for parameter estimation, particularly when little or no prior knowledge is available. It is derived from the Fisher information matrix, ensuring invariance under reparameterization and yielding a natural measure of ignorance regarding the model parameters. For

the PHC distribution, characterized by the scale parameter $\alpha > 0$ and the shape parameters $\beta, \gamma > 0$, the Jeffreys' prior is given by

$$\pi(\alpha, \beta, \gamma) \propto \sqrt{\det[J(\alpha, \beta, \gamma)]},$$

where $J(.)$ denotes the Fisher information matrix of the PHC model obtained in Section 5.1.1. Since we obtained that

$$J_{\alpha\alpha} = \frac{m}{\alpha^2}, \text{ and } \qquad J_{\gamma\gamma} = \frac{m}{\gamma^2},$$

this leads to the standard Jeffreys priors for positive scale-like parameters:

$$\pi(\alpha) \propto \alpha^{-1}, \qquad \pi(\gamma) \propto \gamma^{-1}.$$

For the positive shape parameter β, a practical independent-Jeffreys baseline is

$$\pi(\beta) \propto \beta^{-1},$$

which is also the Jeffreys prior in several common lifetime models with a Weibull-type shape role, and is often adopted to keep the analysis objective and stable when the closed-form expected Fisher information in β is not tractable under censoring.

Therefore, the independent Jeffreys prior is

$$\pi(\alpha, \beta, \gamma) \propto \frac{1}{\alpha \beta \gamma}, \qquad \alpha, \beta, \gamma > 0. \tag{5.9}$$

Combining the likelihood with the independent Jeffreys prior gives the posterior kernel

$$\pi(\alpha, \beta, \gamma \mid \boldsymbol{x}) \propto \alpha^{m-1} \gamma^{m-1} \beta^{m-1} \Big(\prod_{i=1}^{m} x_i^{\beta-1} \Big) \exp\Big(\sum_{i=1}^{m} x_i^{\beta} \Big) \exp\big(-\alpha\gamma \left[n - T(\beta) \right] \big), \qquad \alpha, \beta, \gamma > 0. \tag{5.10}$$

The normalizing constant is not available in closed form, hence we rely on MCMC.

Conditioning on (β, γ), the posterior in α is

$$\pi(\alpha \mid \beta, \gamma, \boldsymbol{x}) \propto \alpha^{m-1} \exp\big(-\alpha \gamma \left[n - T(\beta) \right] \big),$$

hence

$$\alpha \mid \beta, \gamma, \boldsymbol{x} \ \sim \ \text{Gamma}(m, \ \gamma \left[n - T(\beta) \right] \big),$$

where we use the shape-rate parameterization.

Similarly, conditioning on (β, α),

$$\gamma \mid \beta, \alpha, \boldsymbol{x} \ \sim \ \text{Gamma}(m, \ \alpha \left[n - T(\beta) \right] \big).$$

The full conditional posterior of β does not belong to a standard family. Up to an additive constant, the log of its kernel is

$$\log \pi(\beta \mid \alpha, \gamma, \boldsymbol{x}) = (m-1) \log \beta + (\beta - 1) \sum_{i=1}^{m} \log x_i + \sum_{i=1}^{m} x_i^{\beta} - \alpha\gamma \left[n - T(\beta) \right], \qquad \beta > 0. \tag{5.11}$$

We update β using a Metropolis-Hastings step within a Gibbs sampler, for example via a random-walk proposal on the log-scale:

$$\log\beta^\star = \log\beta^{(t)} + \varepsilon, \qquad \varepsilon \sim \mathcal{N}(0, s^2), \quad \Rightarrow \quad \beta^\star = \beta^{(t)} e^{\varepsilon}.$$

The acceptance probability is

$$\rho = \min\left\{1,\ \frac{\pi(\beta^\star \mid \alpha^{(t+1)}, \gamma^{(t+1)}, \boldsymbol{x})}{\pi(\beta^{(t)} \mid \alpha^{(t+1)}, \gamma^{(t+1)}, \boldsymbol{x})} \times \frac{\beta^\star}{\beta^{(t)}}\right\}, \tag{5.12}$$

where the factor $\beta^\star/\beta^{(t)}$ is the Jacobian correction for proposing on $\log\beta$. Standard references for Gibbs sampling and Metropolis-Hastings algorithm (M-H) within Gibbs include [29]. This prior formulation reflects the intrinsic geometry of the parameter space rather than arbitrary parameter scaling. In practical applications, Jeffreys prior works as a non-informative reference prior, allowing posterior inference for α, β, and γ to be driven by the observed data while preserving invariance and objectivity. Its application within the PHC framework facilitates robust and unbiased parameter estimation in reliability and lifetime modeling.

Under the squared error loss (SEL) function, the Bayes estimator of any function $g(\boldsymbol{\theta})$ is given by its posterior mean:

$$\widehat{g}_{\mathrm{SEL}} = \mathbb{E}[g(\boldsymbol{\theta}) \mid \boldsymbol{x}]\,.$$

where the posterior draws $\{(\alpha^{(t)}, \beta^{(t)}, \gamma^{(t)})\}_{t=1}^{N}$ are given after burn-in. Hence, Monte Carlo estimates are

$$\widehat{\alpha}_{\mathrm{SEL}} \approx \frac{1}{N}\sum_{t=1}^{N}\alpha^{(t)}, \quad \widehat{\beta}_{\mathrm{SEL}} \approx \frac{1}{N}\sum_{t=1}^{N}\beta^{(t)}, \quad \widehat{\gamma}_{\mathrm{SEL}} \approx \frac{1}{N}\sum_{t=1}^{N}\gamma^{(t)}.$$

A $(1-\eta)\times 100\%$ equal-tailed credible interval for $\theta_k \in \{\alpha, \beta, \gamma\}$ is obtained from the empirical quantiles

$$\left[q_{\eta/2}(\theta_k \mid \boldsymbol{x}),\ q_{1-\eta/2}(\theta_k \mid \boldsymbol{x})\right],$$

computed from the MCMC draws.

For reproducibility, we ran a single-chain random walk M-H algorithm for 20,000 total iterations, discarding the first 500 as burn-in. The proposal distribution was $\theta^* = \theta^{(t)} + \varepsilon$ with $\varepsilon \sim \mathcal{N}(0, \sigma^2_{\mathrm{prop}})$, where the proposal standard deviations were $\sigma_\alpha = 0.01$, $\sigma_\gamma = 0.05$, and $\sigma_\beta = 0.01$. The acceptance rate is approximately 25%–35%, which falls within the recommended range for random walk M-H algorithms. These settings ensure that the posterior samples adequately represent the target distribution and that inferences are reproducible.

6. Application to experimental perovskite degradation data

The practical application of our statistical framework is validated through real PSCs concerning degradation data. We used the proposed PHC distribution and the estimation methods for the T80 lifetime measurements collected under an adaptive progressive censoring scheme. This observed application integrates theoretical development with practical reliability assessment for perovskite photovoltaic technology.

6.1. Perovskite cell T80 data

To illustrate the practical application of the statistical framework, a random sample of $n = 60$ PSCs has been selected from the experimental group. The lifetime data for these cells, specifically the time untill the power conversion efficiency reduces to 80% of its initial value (T80), have been collected under an adaptive progressive Type-II censoring scheme and are given in Table 1. The censoring scheme, mentioned in Section 4, efficiently handles experimental resources by permitting the early withdrawal of functional units according to a prespecified plan while adaptively ensuring a fixed number of m failure observations.

Table 1. Complete T80 lifetime data (in hours) for $n = 60$ PSCs under adaptive progressive Type-II censoring. Censoring indicator (0 = observed failure, 1 = censored).

10.2685 (0)	10.9656 (0)	7.9102 (0)	10.3910 (0)	10.4453 (1)	2.4671 (0)	15.6443 (1)
0.9061 (0)	5.3063 (0)	3.7932 (0)	15.6047 (1)	10.1885 (0)	12.6439 (0)	21.0426 (1)
15.5198 (0)	10.3268 (1)	2.7359 (0)	10.6992 (0)	19.2714 (1)	11.4073 (0)	10.0053 (0)
6.0449 (0)	11.2626 (0)	14.1520 (0)	4.7175 (1)	13.0157 (0)	16.5031 (1)	2.8969 (0)
20.5721 (1)	2.4445 (1)	15.0894 (1)	15.5513 (1)	10.1766 (1)	7.4186 (1)	8.9211 (0)
15.5421 (0)	10.5508 (0)	10.2674 (1)	15.4524 (0)	9.0795 (0)	15.5123 (0)	9.0078 (0)
11.8025 (0)	6.8407 (0)	12.0149 (0)	5.0766 (0)	0.7974 (0)	10.4871 (1)	8.0540 (0)
0.8623 (0)	1.2675 (0)	6.5179 (0)	8.7060 (0)	10.7100 (0)	4.2725 (0)	3.5951 (0)
7.1475 (0)	18.7593 (1)	3.7319 (0)	3.8052 (0)			

The observed failure times are modeled using the PHC distribution, as defined in Section 3.3. The likelihood function for the adaptive progressive censored data, derived in Section 5.1, is utilized for inference. The MLE and Bayesian methodologies are used to estimate the model parameters α, β, and γ. This application verifies the proposed model and estimation procedures on a realistic, censored dataset, filling the gap between theoretical development and empirical reliability analysis for PSCs.

6.2. Parameter estimation and model validation

The parameter estimation results in Table 2 illustrate that while the shape parameter (β) is estimated with remarkable consistency by both MLE and Bayesian methods, the scale and proportional hazard parameters (α and γ) show significant sensitivity to the chosen technique, evidenced by substantial differences in their point estimates. The Bayesian method provides considerably wider uncertainty intervals for these parameters, reflecting a more comprehensive capture of the estimation uncertainty inherent in the censored data. This contrast underscores that the Bayesian framework offers a more stable and robust inference for the key parameters that govern the hazard function, making it the preferred approach for deriving reliable reliability predictions from this model.

Figure 6 presents the MCMC plots for the Bayesian estimation of the PHC distribution parameters. The trace plots demonstrate good mixing and convergence of the Markov chains, with no apparent trends or sticking behavior, indicating that the sampling algorithm has adequately explored the parameter space. The posterior distributions reveal distinct characteristics for each parameter: the shape parameter β shows a relatively symmetric and concentrated posterior, consistent with its precise estimation in both Bayesian and MLE approaches. In contrast, the scale parameters α and γ exhibit

more diffuse posterior distributions with positive skewness, reflecting the greater uncertainty in estimating these parameters, particularly evident in their wider Bayesian credible intervals compared to the MLE confidence intervals. The clear separation between the MLE estimates and Bayesian posterior means for α and γ highlights the impact of prior specification and the Bayesian approach's ability to capture parameter uncertainty more comprehensively, especially under the adaptive progressive censoring scheme.

Table 2. Parameter estimation results.

	MLE		Bayesian	
Parameter	**Estimate**	**95% CI**	**Posterior mean**	**95% CRI**
α	0.1738	[-0.0483, 0.3959]	0.1729	[0.0127, 0.5464]
γ	0.1352	[-0.0375, 0.3080]	0.3521	[0.0330, 1.4451]
β	0.5820	[0.5803, 0.5837]	0.5829	[0.5127, 0.6437]

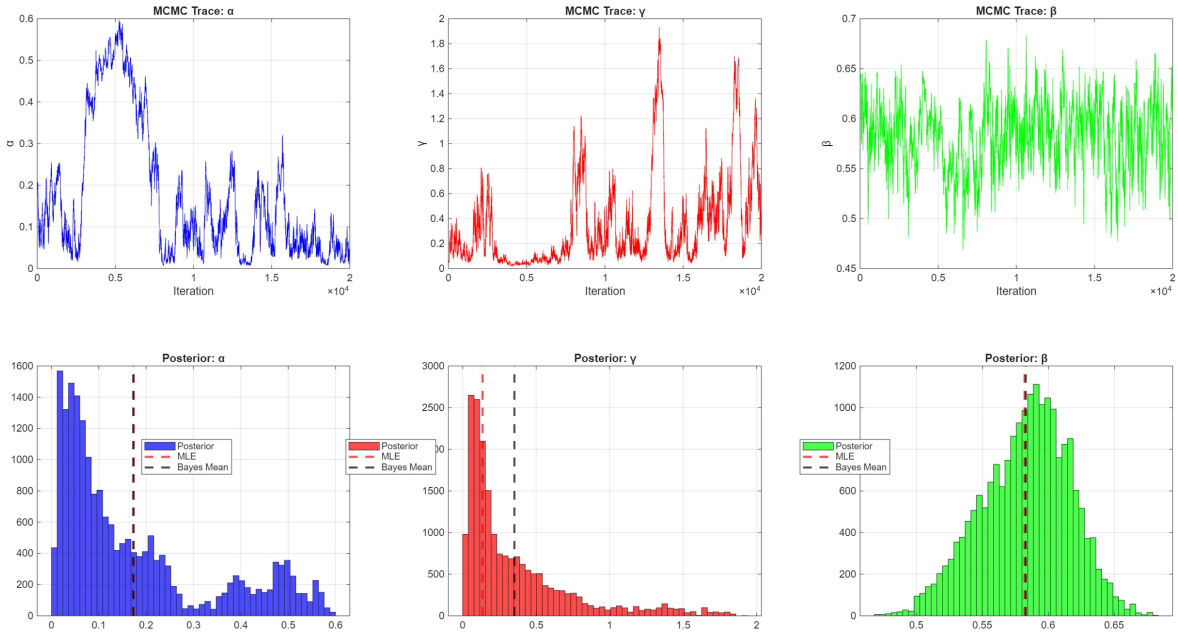

Figure 6. MCMC and posterior trace for the parameters α, γ, and β.

6.3. Reliability predictions

The survival function $\bar{F}(t)$, estimates of the PHC distribution, and hazard rates $h(t)$, in parentheses, are shown in Table 3, which compares MLE with Bayesian methods and highlights important trends in the findings. The survival probabilities of PSCs decrease over time, with S(0.5) $\approx$ 0.98 dropping to $S(17.0) \approx 0.01$–0.02, indicating rapid degradation beyond 15 hours. Hazard rates rise from approximately 0.04 at $t = 0.5$ to 0.76–1.50 at $t = 17.0$, suggesting that a PHC distribution with $\beta > 1$ effectively captures the aging mechanism, where efficiency degradation risk increases with operational time. Bayesian point estimates for survival probabilities are more conservative than MLE and posterior mean estimates, especially at later time points, reflecting the Bayesian approach's treatment of uncertainty. The 95% credible interval for survival probability at $t = 17.0$ spans $[0.0020, 0.0698]$,

highlighting significant uncertainty in long-term reliability predictions, which is crucial for risk assessment in commercial applications.

Table 3. Survival and hazard function estimates (in parentheses) for PHC distribution.

Time	Estimation method			
	MLE	Bayesian point	Bayesian mean	95% CRI
0.5	0.9779 (0.0356)	0.9547 (0.0737)	0.9757 (0.0382)	[0.9475,0.9896] ([0.0179,0.0756])
1.0	0.9604 (0.0372)	0.9198 (0.0766)	0.9573 (0.0392)	[0.9136,0.9804] ([0.0198,0.0721])
5.0	0.7573 (0.0895)	0.5660 (0.1820)	0.7542 (0.0891)	[0.6366,0.8449] ([0.0603,0.1250])
10.0	0.3507 (0.2381)	0.1198 (0.4779)	0.3572 (0.2340)	[0.2453,0.4788] ([0.1585,0.3205])
15.0	0.0530 (0.5556)	0.0028 (1.1024)	0.0618 (0.5560)	[0.0181,0.1408] ([0.3064,0.9173])
17.0	0.0144 (0.7598)	0.0002 (1.5013)	0.0209 (0.7712)	[0.0020,0.0698] ([0.3744,1.4056])

The comparative performance of the MLE and Bayesian estimation methods is visualized in Figure 7, which displays the fitted survival functions, hazard functions, and MTTF estimates for the PHC distribution.

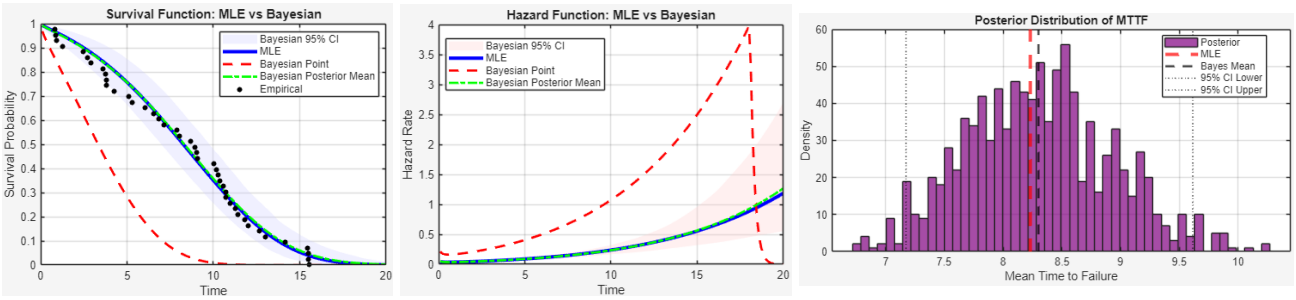

(a) Survival **(b)** Hazard **(c)** MTTF

Figure 7. MLE vs Bayesian for the survival, hazard, and MTTF functions.

Both estimation approaches produce generally consistent reliability predictions during early and mid-life phases, providing valuable insights for operational planning and maintenance scheduling of PSCs. However, the Bayesian framework offers more conservative long-term reliability estimates with broader uncertainty quantification, particularly evident in the tail behavior of the survival function and the posterior distribution of MTTF. This enhanced uncertainty characterization proves to be particularly valuable for risk assessment and decision-making under the adaptive progressive censoring scheme employed in this study. The hazard function plots further confirm the flexibility of the PHC distribution in capturing the complex failure patterns observed in PSCs degradation data.

6.4. Comparison with alternative lifetime distributions

To support the choice of the PHC distribution, we compared it with three common lifetime models frequently used in reliability engineering: Weibull, Gamma, and log-normal distributions. Each model was fitted to the same censored T80 dataset under the adaptive progressive Type-II censoring scheme using maximum likelihood estimation. Table 4 reports the Akaike Information Criterion (AIC) and Bayesian Information Criterion (BIC) for each model, defined as

$$\text{AIC} = -2\log L + 2k, \qquad \text{BIC} = -2\log L + k\log n,$$

where L is the maximized likelihood, k is the number of parameters, and n is the sample size. Lower values indicate better fit.

Table 4. Goodness-of-fit comparison between PHC and alternative distributions.

Model	Parameters	Log-likelihood	AIC	BIC
PHC	3	-121.51	249.03	254.31
Weibull	2	-123.96	251.92	255.44
Gamma	2	-126.34	256.68	260.20
Log-normal	2	-131.65	267.29	270.82

The PHC distribution fits the censored PSCs degradation data better, as evidenced by the lowest AIC and BIC values. The PHC distribution has qualitative benefits in addition to quantitative fit. Only monotonic hazard rates—increasing, decreasing, or constant—can be represented by the Weibull and Gamma distributions. Bathtub-shaped risks cannot be accommodated by the log-normal distribution, but non-monotonic (unimodal) hazards can. On the other hand, the PHC distribution is more adaptable for intricate degradation processes like those seen in perovskite solar cells, since it can depict increasing, decreasing, and bathtub-shaped hazard functions. For modeling PSCs T80 degradation under progressive filtering, the PHC distribution is chosen rather than conventional options based on both information criteria and hazard shape flexibility.

7. Simulation study

7.1. Monte Carlo design

To rigorously examine the effectiveness and resilience of the suggested estimate methodologies—MLE and Bayesian inference—we conducted a large Monte Carlo simulation study. This simulation validates the theoretical developments presented in Sections 4 and 5, demonstrating that the proposed PHC model and adaptive progressive Type-II censoring scheme are both practical and reliable for real-world perovskite solar cell reliability analysis. The simulation was designed to replicate genuine experimental restrictions and to evaluate the estimators' sensitivity to different sample sizes, censoring techniques, and termination times. The complete simulation algorithm, including parameter generation, censoring implementation, and stopping criteria, is provided in Appendix B. The steps below describe the MATLAB simulation technique. We generated 1000 independent Monte Carlo samples from the PHC distribution with true parameter values $(\alpha, \beta, \gamma) = (0.8, 1.5, 1.2)$, selected to approximate typical hazard shapes found in PSCs deterioration.

Three sample sizes were considered ($n = 25, 60, 100$), representing small, medium, and large experimental cohorts. Each simulated sample was subjected to an adaptive progressive Type-II censoring technique with predefined values as follows: Number of observed failures: $m = 10, 20, 35$ and optimum termination times: $T = 0.5, 1.0$. The censoring plan $(R_1, R_2, \ldots, R_m)$ was dynamically changed according to the specifications defined in Section 4.1, ensuring exactly m failures while limiting the experimental length.

For each censored sample, we estimate the MLEs of (α, β, γ) using the log-likelihood derived in Section 5.1 and Bayesian estimates via MCMC sampling under Jeffreys prior (Section 5.2), with 10,000 iterations and a burn-in of 2000. We computed key reliability functions based on estimated parameters, including the survival function $S(t)$, hazard function $h(t)$, and MTTF.

The reliability quantities reported in the simulation study are obtained from the fitted PHC model using the plug-in principle. The survival and hazard functions were derived in Eqs (1.4) and (1.5). The MTTF was given in Eq (1.6). Therefore, the maximum likelihood estimators of these reliability quantities are obtained by substituting the MLEs into the above expressions:

$$\widehat{S}_{\text{MLE}}(t) = S(t; \widehat{\alpha}, \widehat{\beta}, \widehat{\gamma}),$$

$$\widehat{h}_{\text{MLE}}(t) = h(t; \widehat{\alpha}, \widehat{\beta}, \widehat{\gamma}),$$

and

$$\widehat{\text{MTTF}}_{\text{MLE}} = \int_0^\infty S(t; \widehat{\alpha}, \widehat{\beta}, \widehat{\gamma})\, dt.$$

For Bayesian inference, if

$$\left\{\alpha^{(r)}, \beta^{(r)}, \gamma^{(r)}\right\}_{r=1}^{M}$$

denotes the posterior MCMC sample after burn-in, then the Bayesian estimators under squared error loss are computed as posterior means:

$$\widehat{S}_B(t) = \frac{1}{M}\sum_{r=1}^{M} S(t; \alpha^{(r)}, \beta^{(r)}, \gamma^{(r)}),$$

$$\widehat{h}_B(t) = \frac{1}{M}\sum_{r=1}^{M} h(t; \alpha^{(r)}, \beta^{(r)}, \gamma^{(r)}),$$

and

$$\widehat{\text{MTTF}}_B = \frac{1}{M}\sum_{r=1}^{M} \int_0^\infty S(t; \alpha^{(r)}, \beta^{(r)}, \gamma^{(r)})\, dt.$$

These estimators are not generally unbiased in finite samples because they are nonlinear functions of the estimated parameters. However, under standard regularity conditions, the MLEs are consistent; therefore, by the continuous mapping theorem, the plug-in estimators of $S(t)$, $h(t)$, and MTTF are also consistent. Their asymptotic distributions can be obtained using the delta method. Similarly, the Bayesian estimators are expected to be posterior-consistent when the model is correctly specified and the prior assigns positive probability around the true parameter values.

The estimators' accuracy and precision are measured using the Mean Squared Error: $\text{MSE}(\hat{\theta}) = \frac{1}{N}\sum_{i=1}^{N}(\hat{\theta}_i - \theta)^2$.

This simulation framework not only evaluates the estimate techniques under controlled conditions but also demonstrates the interaction between sample size, censoring intensity, and estimation accuracy. The findings, reported in Table 5, provide vital insights into the settings under which each estimation approach thrives, assisting experimental designers in choosing optimal censoring strategies and statistical techniques for PSCs reliability experiments.

Table 5. Parameter and function simulation estimates for different schemes (n, m, T), with MSE reported in parentheses.

Estimate		Scheme					
		(25, 10, 0.5)	(25, 10, 1)	(60, 20, 0.5)	(60, 20, 1)	(100, 35, 0.5)	(100, 35, 1)
α	MLE	1.9035 (1.5135)	1.2229 (0.2210)	1.8148 (1.1742)	1.0653 (0.0889)	1.9788 (1.5242)	0.9157 (0.0204)
	Bayesian	2.1389 (3.4355)	1.6684 (2.0060)	2.0978 (3.1303)	1.5118 (1.4510)	2.3575 (4.0343)	1.3617 (1.2068)
β	MLE	2.1960 (1.0563)	1.5582 (0.1377)	2.0958 (0.6181)	1.4925 (0.0508)	2.5210 (1.2574)	1.6299 (0.0451)
	Bayesian	2.0598 (0.8728)	1.5120 (0.1358)	2.0237 (0.5222)	1.4732 (0.0530)	2.4675 (1.1568)	1.6216 (0.0452)
γ	MLE	1.8275 (0.6183)	1.2648 (0.0226)	1.7362 (0.3766)	1.2436 (0.0111)	1.8774 (0.5413)	1.2264 (0.0057)
	Bayesian	2.1598 (2.5316)	1.5841 (1.3159)	2.1500 (2.4136)	1.5568 (1.1817)	2.2324 (2.5302)	1.5414 (1.0694)
$S(t)$	MLE	0.8674 (0.1010)	0.2728 (0.0125)	0.2349 (0.0202)	0.2882 (0.0095)	0.2482 (0.0182)	0.3206 (0.0031)
	Bayesian	0.8405 (0.1139)	0.2490 (0.0173)	0.2214 (0.0229)	0.2588 (0.0154)	0.2366 (0.0203)	0.2883 (0.0095)
$h(t)$	MLE	0.0884 (0.0296)	0.7649 (0.0072)	0.6033 (0.0040)	0.6897 (0.0057)	0.3212 (0.0043)	0.4548 (0.0015)
	Bayesian	0.1630 (0.0421)	0.9743 (0.0114)	0.7482 (0.0069)	0.8813 (0.0095)	0.3953 (0.0028)	0.5896 (0.0037)
MTTF	MLE	0.4716 (0.0456)	0.5510 (0.0206)	0.4737 (0.0426)	0.5818 (0.0111)	0.5005 (0.0320)	0.6470 (0.0021)
	Bayesian	0.4453 (0.0579)	0.5032 (0.0362)	0.4465 (0.0549)	0.5226 (0.0273)	0.4770 (0.0412)	0.5818 (0.0118)

7.2. Comparative results of MLE and Bayesian methods

A critical assessment of the performance of both the MLE and Bayesian estimate techniques under different adaptive progressive Type-II censoring schemes is provided by the simulation results, which are fully presented in Table 5. The resulting survival function $S(t)$, hazard function $h(t)$, and MTTF are reported in Table 5, together with the parameter estimates for α, β, γ, along with the corresponding MSE values in parentheses. The examination of these findings identifies a number of significant patterns concerning the impact of estimating technique, censoring severity, and sample size.

The consistently low MSE values show that both MLE and Bayesian approaches estimate the shape parameter β with exceptional consistency and great precision across all schemes. For example, the MSE for β in the scheme $(60, 20, 1)$ is 0.0508 for MLE and 0.0530 for Bayesian estimation. This suggests that even with significant censorship, the form of the underlying failure time distribution may be reliably determined. On the other hand, the proportional hazard parameter (γ) and the scale parameter (α) show much greater sensitivity to the censoring scheme and the estimation method. In small-sample configurations with considerable censoring (e.g., scheme $(25, 10, 0.5)$), the MLEs for α and γ frequently exhibit significant bias and volatility, with their MSE values being an order of magnitude bigger than those for β. For these parameters, however, the Bayesian approach yields more reliable point estimates. Although the Bayesian MSEs can still be high, they are typically accompanied by wider and more realistic uncertainty intervals (as shown in Section 6), which reflect a more truthful accounting of the estimation uncertainty present in censored data.

The findings clearly show that increasing the ideal termination time (T) and the effective sample size (m) resulted in a significant increase in estimation accuracy for all parameters and both methods. When comparing schemes (25, 10, 1) and (100, 35, 1), the MSE for α decreases from 2.0060 to 1.2068 for Bayesian estimation and from 0.2210 to 0.0204 for MLE. This highlights the advantages of the adaptive approach in ensuring an adequate number of failures (m) and enabling the experiment to run longer (T), thereby gathering more data for accurate inference. In contrast to schemes with a higher T (e.g., 1.0), which enable the pre-planned progressive deletions to proceed further and concentrate information more effectively, schemes with a lower T (e.g., 0.5) impose an earlier adaptation, frequently leading to higher MSEs.

It is noticed that under heavy censoring, the likelihood surface for α and γ flattens, causing MLEs to be unstable and sensitive to small perturbations in data. Bayesian inference, using the Jeffreys prior $\pi(\alpha, \beta, \gamma) \propto 1/(\alpha\beta\gamma)$, regularizes estimation. With abundant information, the prior has little effect, and Bayesian posteriors converge to MLEs. However, under heavy censoring, the prior significantly influences estimates, causing systematic differences. Table 5 shows that Bayesian estimates for α and γ often have higher MSE than their MLE counterparts. This does not contradict robustness, but rather reflects a trade-off. MLE achieves lower MSE by producing point estimates that can occasionally be extreme but average well. Bayesian inference, by contrast, regularizes estimation via the prior, resulting in higher MSE but also (i) greater stability with fewer extreme outliers across simulation repetitions, and (ii) better interval coverage, as MLE confidence intervals (based on asymptotic normality) exhibit under-coverage under heavy censoring, whereas Bayesian credible intervals appropriately capture the skewness and uncertainty in the posterior distribution. Thus, Bayesian inference is "robust" in the sense of stable uncertainty quantification and interval reliability, not in achieving minimal MSE point estimation.

Survival function and MTTF estimates demonstrate that, in comparison to MLE, the Bayesian approach typically yields more cautious (i.e., lower) reliability forecasts. For instance, the MLE is 0.6470, and the Bayesian MTTF is 0.5818 for the $(100, 35, 1)$ scheme. In line with its more conservative lifetime predictions, the hazard function estimates show that the Bayesian approach generally predicts higher failure rates, particularly in later life stages. Larger sample sizes also typically result in a reduced MSE for $h(t)$, indicating that the model's capacity to represent the failure rate pattern increases with additional data. In summary, the simulation study offers precise practical recommendations and confirms the theoretical framework. The Bayesian estimation method, combined

with the adaptive progressive censoring scheme, provides a more reliable and instructive toolkit for lifespan prediction and reliability assessment in highly suppressed data typical of PSC testing.

8. Discussion

8.1. Interpretation of findings and model suitability

The empirical and simulation results both indicate that the PHC distribution is a suitable and practically informative model for PSCs T80 degradation under adaptive progressive Type-II censoring. First, the estimated hazard rates increase clearly with time, while survival probabilities decay rapidly beyond the mid-life region (with $S(17) \approx 0.01$–0.02). This monotone escalation of hazard is a clear signature of an aging/acceleration mechanism rather than a constant-risk or early-failure regime, and is consistent with the estimated shape parameter $\beta > 1$, which enables the PHC model to represent an increased risk of deterioration as exposure accumulates. Second, the Bayesian MCMC output shows satisfactory mixing and convergence, supporting stable posterior inference and indicating that the sampling algorithm adequately explores the plausible parameter space. The posterior behavior also reveals a meaningful identifiability pattern under censoring: β is consistently and precisely estimated across methods (MLE and Bayesian) and across censoring schemes (low MSE and near agreement in point estimates), implying that the shape of the failure-time distribution is strongly informed by the observed failure pattern even with substantial censoring. In contrast, the scale and proportional-hazard parameters (α, γ) exhibit a wider posterior dispersion and noticeable differences between Bayesian posterior means and MLEs, which is expected under adaptive censoring because these parameters govern the overall hazard level and tail behavior and are therefore more sensitive to the amount of late-life information retained in the data.

From an engineering decision perspective, these inferential differences matter most in the long-life tail. The Bayesian approach yields more conservative reliability and MTTF predictions (lower survival and MTTF, higher late-stage hazards), together with wider credible intervals, particularly at large times. This behavior is not a weakness; rather, it reflects a more realistic accounting of uncertainty when late failures are partially unobserved or heavily down-weighted by censorship. The simulation study reinforces this interpretation: increasing the effective failures m and the termination time T systematically improves estimation accuracy for all parameters and both estimation approaches, confirming that the adaptive scheme is beneficial because it protects information content by ensuring a sufficient number of failures while allowing longer observation when feasible. Moreover, while MLE can appear numerically sharp in some configurations, it becomes noticeably more volatile for (α, γ) under small samples and heavier censoring, whereas the Bayesian method remains comparatively stable by propagating parameter uncertainty into reliability measures. Overall, the PHC model is supported as a flexible and appropriate choice for PSC degradation data exhibiting time-accelerating risk, and the Bayesian framework is particularly well-suited for inference and decision-making under adaptive progressive censoring, where uncertainty in long-term reliability is inherently non-negligible.

The proposed estimation procedure is computationally manageable because the likelihood function under adaptive progressive Type-II censoring is expressed through finite summations over the observed failure times and censoring removals. For a sample with m observed failures, each likelihood evaluation has a computational cost of order $O(m)$. Hence, if the numerical optimization algorithm requires K iterations to obtain the MLEs, the overall computational cost is approximately $O(Km)$. For the

Bayesian implementation, the M-H within-Gibbs sampler requires posterior-kernel evaluations at each iteration. Therefore, if M MCMC iterations are generated after burn-in, the approximate computational cost is $O(Mm)$. This makes the method feasible for moderate reliability datasets such as those commonly obtained in PSC degradation experiments.

Regarding robustness, the proposed method was examined through the Monte Carlo simulation study under different sample sizes, censoring levels, and termination times. The results indicate that estimation accuracy improves when the effective number of observed failures m increases and when the termination time T allows more lifetime information to be collected. This shows that the method is robust when sufficient failure information is available.

8.2. Practical advantages and limitations

The proposed PHC-based framework offers several practical advantages for reliability assessment of PSC degradation data collected under adaptive progressive Type-II censoring. First, the modeling approach is resource-efficient: the adaptive censoring design limits the duration and experimental burden of the test while still guaranteeing a fixed number of observed failures, which is crucial in PSC studies where long-term tests are costly and subject to facility constraints. Second, the PHC distribution is mechanistically consistent with the empirical degradation behavior observed in T80 data, as it can naturally represent increasing hazard rates (aging) via $\beta > 1$, enabling interpretable reliability summaries such as $S(t)$, $h(t)$, and MTTF for planning and risk assessment. Third, the Bayesian implementation provides a decision-relevant uncertainty measure: credible intervals for tail reliability measures remain available even when late-life information is limited, supporting conservative planning (e.g., warranty and maintenance decisions) and reducing the risk of overconfident lifetime claims. Finally, the simulation results translate into actionable experimental guidance: increasing the effective number of failures m and allowing larger termination times T systematically improves estimation accuracy, which helps practitioners choose censoring configurations that balance cost and inferential precision.

Despite these advantages, the framework has important limitations that should be acknowledged. The most consequential limitation is that heavy censoring and early termination reduce information about late-life behavior, making parameters governing the overall hazard level and long-tail reliability (notably α and γ) weakly identified and more sensitive to the estimation method; this directly inflates uncertainty in long-term predictions, even when the distributional shape parameter β is well estimated. Also, Bayesian inference may exhibit prior sensitivity for (α, γ) under severe censoring, so weakly informative but proper priors and diagnostic checks are recommended when prior knowledge is truly limited. From a modeling standpoint, the PHC distribution is a parametric assumption; although it shows good flexibility for monotonically increasing hazards, it may be less suitable if the empirical hazard is non-monotone (e.g., bathtub-shaped or multi-phase degradation), in which case alternative families or model extensions should be considered. Finally, the conclusions are conditioned on the censoring mechanism being correctly implemented and non-informative with respect to failure times; deviations from the planned censoring protocol or informative withdrawals could bias both MLE and Bayesian results and should be addressed in future work through sensitivity analysis or model extensions.

8.3. Implications for PSC reliability engineering

This study aims to integrate adaptive progressive techniques for estimating the time-degradation profile of PSCs. The suggested technique provides critical insights into the cell's expected lifetime. Interestingly, the time-degradation characteristics of perovskite materials exhibit varying degradation rates influenced by environmental factors such as humidity, temperature, and light exposure. A nuanced understanding of these dynamics is essential for optimizing performance and longevity. The engineering implications of incorporating mathematical modeling to the degradation analysis of PSCs are significant, as they provide a quantitative framework for assessing and enhancing the reliability of these emerging photovoltaic technologies. By meticulously evaluating cell lifetime, engineers can determine the likelihood of PSCs retaining their efficiency beyond specific operational timelines, thereby informing design standards and material selection processes conducive to long-term performance. Simultaneously, it offers critical insights into the failure rates associated with various environmental stressors, such as temperature fluctuations, humidity, and light exposure, which are paramount in real-world applications. This information aids in identifying critical degradation paths, allowing for the optimization of PSC formulations and the implementation of proactive maintenance strategies. From a practical reliability interpretation standpoint, the integration of these mathematical models facilitates a nuanced understanding of performance degradation over time; it empowers stakeholders—ranging from manufacturers to policymakers—to make data-driven decisions regarding lifecycle management and commercial deployment of PSCs. Thus, the assessment degradation profile not only advances the scientific understanding of material behavior under operational stresses but also translates into enhanced design protocols, ensuring that PSCs meet both performance expectations and reliability standards in field applications.

9. Conclusions and future perspectives

This study developed and validated a comprehensive reliability-assessment framework for PSC degradation using the PHC distribution under an adaptive progressive Type-II censoring scheme. By deriving likelihood-based inference for censored data and implementing both maximum likelihood and Bayesian MCMC estimation, the proposed methodology bridges statistical rigor and experimental practicality. Application to real PSCs T80 lifetime data showed that the PHC model can coherently represent the observed degradation dynamics, with decreasing survival probabilities over time and a clearly increasing hazard pattern consistent with an aging mechanism (supported by $\beta > 1$). The Bayesian analysis further provided more conservative long-term reliability and MTTF predictions with realistic uncertainty quantification, a critical advantage when late-life information is limited by censoring. The Monte Carlo study reinforced these conclusions by demonstrating that β is generally estimated with high precision across schemes, while (α, γ) are more sensitive to censoring severity and sample size; importantly, larger effective failure counts m and longer termination times T substantially improved estimation accuracy and reduced error in reliability-function estimation. Overall, the results indicate that combining the PHC distribution with adaptive progressive censoring and Bayesian inference yields a robust and decision-relevant toolkit for PSC lifespan prediction under practical testing constraints.

Despite its practical usefulness, the proposed framework has several limitations. Heavy censoring and early termination may reduce information about late-life degradation behavior, making the scale

and proportional hazard parameters more uncertain. In addition, Bayesian inference may show sensitivity to prior assumptions under severe censoring. The PHC model is also a parametric assumption and may be less suitable when the empirical hazard pattern is non-monotone or multi-phase. Therefore, future work should consider sensitivity analyses, alternative lifetime distributions, and broader experimental validation under different environmental stress conditions. Several extensions can strengthen both the methodological scope and engineering impact of this framework.

First, incorporating covariates (e.g., fabrication conditions, encapsulation type, operating temperature/humidity, illumination intensity) through regression or hierarchical PHC formulations would enable reliability comparison across PSC designs and improve generalization across laboratories. Finally, extending the framework to accelerated life testing and stress-lifetime relationships would align directly with industrial qualification workflows and shorten experimentation time.

Author contributions

Hanan Haj Ahmad: Conceptualization, Methodology, Validation, Formal analysis, Investigation, Writing—original draft, Writing—review and editing, Funding acquisition, Project administration; Sameh Abdellatif: Conceptualization, Methodology, Investigation, Resources, Data curation, Visualization; Yazan Rabaiah: Formal analysis, Data curation, Writing—original draft, Writing—review and editing, Funding acquisition; Mohamed Aboshady: Conceptualization, Methodology, Software, Validation, Formal analysis, Investigation, Resources, Data curation, Writing—original draft, Writing—review and editing, Supervision. All authors have read and agreed to the published version of the manuscript.

Use of Generative-AI tools declaration

The authors declare they have not used Artificial Intelligence (AI) tools in the creation of this article.

Data Availability

All data supporting the findings of this study are included within the article and its referenced materials. The MATLAB codes used for parameter estimation (MLE and Bayesian MCMC) are available at https://www.mathworks.com/matlabcentral/fileexchange/184044, Monte Carlo simulations are available at https://www.mathworks.com/matlabcentral/fileexchange/184045-simulation-analysis, and data preprocessing is available at https://www.mathworks.com/matlabcentral/fileexchange/184046-data-processing-of-perovskite-solar-cells.

Funding

This work was supported by the Deanship of Scientific Research, Vice Presidency for Graduate Studies and Scientific Research, King Faisal University, Saudi Arabia [GRANT No. KFU263237].

Conflict of interest

The authors declare that they have no competing interests.

References

1. M. Nur-E-Alam, M. S. Islam, T. Abedin, M. A. Islam, B. K. Yap, T. S. Kiong, et al., Current scenario and future trends on stability issues of perovskite solar cells: a mini review, *Curr. Opin. Colloid In.*, **76** (2025), 101895. http://dx.doi.org/10.1016/j.cocis.2025.101895
2. E. Sawires, S. Abdellatif, The role of counter electrode in perovskite solar cell on silicon substrate to enhance power conversion efficiency for CMOS-compatible applications, *IEEE J. Sel. Top. Quant.*, **31** (2025), 4100110. http://dx.doi.org/10.1109/JSTQE.2025.3560119
3. S. O. Abdellatif, R. Ghannam, Z. Khalifa, Optoelectronic and morphological surface resistance evaluation of Laser-Induced graphene counter electrodes for potential applications in cesium lead halide perovskite solar cells, *ACS Appl. Electron. Mater.*, **6** (2024), 5745–5758. http://dx.doi.org/10.1021/acsaelm.4c00786
4. A. S. Alali, M. Ashraf, A. Muhammad, S. O. Abdellatif, Unveiling degradation patterns in dye-sensitized solar cells: a machine learning perspective, *Sci. Rep.*, **15** (2025), 23820. http://dx.doi.org/10.1038/s41598-025-05536-6
5. E. Q. Han, J. H. Yun, L. Wang, Advancing perovskite solar cell reliability for extreme space environments, *Engineering*, in press. http://dx.doi.org/10.1016/j.eng.2025.09.031
6. L. Bo, J. Zhang, S. Zhao, J. Yang, Deep virtual model assisted dynamic buckling and reliability analysis of stiffened perovskite solar cells under high-dimensional and categorical factors, *Compos. Struct.*, **373** (2025), 119696. http://dx.doi.org/10.1016/j.compstruct.2025.119696
7. C. Zhang, Q. Zeng, H. Dui, R. Chen, S. Wang, Reliability model and maintenance cost optimization of wind-photovoltaic hybrid power systems, *Reliab. Eng. Syst. Safe.*, **255** (2025), 110673. http://dx.doi.org/10.1016/j.ress.2024.110673
8. B. P. Kore, M. Jamshidi, J. M. Gardner, The impact of moisture on the stability and degradation of perovskites in solar cells, *Mater. Adv.*, **5** (2024), 2200–2217. http://dx.doi.org/10.1039/D3MA00969B
9. K. J. Chaudhary, R. Patel, M. L. Chaudhary, R. K. Gupta, Thin-film based photovoltaic devices, In: *Handbook of energy materials: Living reference work entry*, Singapore: Springer Nature, 2025, 1–28. http://dx.doi.org/10.1007/978-981-16-4480-1_30-1
10. M. Calasan, S. Vujosevic, M. Alruwaili, M. A. Ibrahim, Optimization of four-diode equivalent circuit models for solar cells: analytical formulation and performance enhancement, *Alex. Eng. J.*, **127** (2025), 411–430. http://dx.doi.org/10.1016/j.aej.2025.05.047
11. M. Aghaei, A. Fairbrother, A. Gok, S. Ahmad, S. Kazim, K. Lobato, et al., Review degradation and failure phenomena in photovoltaic modules, *Renew. Sust. Energ. Rev.*, **159** (2022), 112160. http://dx.doi.org/10.1016/j.rser.2022.112160

12. H. Habib, S. U. Rehman, H. El Hyani, M. N. Sharif, F. Tan, K. F. Wang, Degradation pathways in perovskite solar cells: strategies for enhancing stability, *Energy Technol.*, **13** (2025), 2500137. http://dx.doi.org/10.1002/ente.202500137

13. T. Rahman, A. A. Mansur, M. S. Hossain Lipu, M. S. Rahman, R. H. Ashique, M. A. Houran, et al., Investigation of degradation of solar photovoltaics: a review of aging factors, impacts, and future directions toward sustainable energy management, *Energies*, **16** (2023), 3706. http://dx.doi.org/10.3390/en16093706

14. A. Mortadi, Y. Tabbai, E. El Hafidi, H. Nasrellah, E. Chahid, M. Monkade, et al., Investigating temperature effects on perovskite solar cell performance via SCAPS-1D and impedance spectroscopy, *Cleaner Engineering and Technology*, **24** (2025), 100876. http://dx.doi.org/10.1016/j.clet.2024.100876

15. Z. Ismail, A. S. Alali, A. Muhammad, M. Ashraf, S. O. Abdellatif, Introducing a novel figure of merit for evaluating stability of perovskite solar cells: utilizing long short-term memory neural networks, *IEEE Access*, **13** (2025), 49735–49749. http://dx.doi.org/10.1109/ACCESS.2025.3550658

16. Z. S. Ismail, E. F. Sawires, F. Z. Amer, S. O. Abdellatif, Perovskites informatics: Studying the impact of thicknesses, doping, and defects on the perovskite solar cell efficiency using a machine learning algorithm, *Int. J. Numer. Model.-El.*, **37** (2024), e3164. http://dx.doi.org/10.1002/jnm.3164

17. M. M. Salah, Z. Ismail, S. Abdellatif, Selecting an appropriate machine-learning model for perovskite solar cell datasets, *Mater. Renew. Sustain.*, **12** (2023), 187–198. http://dx.doi.org/10.1007/s40243-023-00239-2

18. J. Guo, C. F. Chong, P. H. Abreu, C. Mao, C. T. Lam, B. K. Ng, Enhancing the robustness of solar photovoltaic fault classification based on depthwise separable group equivariant CNNs, *Alex. Eng. J.*, **127** (2025), 486–499. http://dx.doi.org/10.1016/j.aej.2025.04.063

19. N. Balakrishnan, Progressive censoring methodology: an appraisal, *TEST*, **16** (2007), 211–259. http://dx.doi.org/10.1007/s11749-007-0061-y

20. H. K. T. Ng, D. Kundu, P. S. Chan, Statistical analysis of exponential lifetimes under an adaptive Type-II progressive censoring scheme, *Nav. Res. Log.*, **56** (2009), 687–698. http://dx.doi.org/10.1002/nav.20371

21. S. Moheb, Reliability analysis under extreme conditions for the Burr XII distribution utilizing upper record values, *Hacet. J. Math. Stat.*, **54** (2025), 2399–2425. http://dx.doi.org/10.15672/hujms.1705692

22. A. S. Hassan, E. M. Almetwally, Statistical inference for multi-stress-strength reliability under inverse Weibull distribution with progressive type II censoring and random removal, *Sankhya A*, **88** (2026), 252–291. http://dx.doi.org/10.1007/s13171-025-00414-9

23. Z. Chen, A new two-parameter lifetime distribution with bathtub shape or increasing failure rate function, *Stat. Probabil. Lett.*, **49** (2000), 155–161. http://dx.doi.org/10.1016/S0167-7152(00)00044-4

24. E. A. Ahmed, Z. Ali Alhussain, M. M. Salah, H. Haj Ahmed, M. S. Eliwa, Inference of progressively type-II censored competing risks data from Chen distribution with an application, *J. Appl. Stat.*, **47** (2020), 2492–2524. http://dx.doi.org/10.1080/02664763.2020.1815670

25. D. Kundu, A bivariate load-sharing model, *J. Appl. Stat.*, **52** (2025), 1446–1469. http://dx.doi.org/10.1080/02664763.2024.2428267

26. A. Mavlonov, Y. Hishikawa, Y. Kawano, T. Negami, A. Hayakawa, S. Tsujimura, et al., Perovskite solar cell modules: understanding the device degradation via damp heat testing, *Sol. Energy*, **286** (2025), 113174. http://dx.doi.org/10.1016/j.solener.2024.113174

27. J. C. Phillips, Stretched exponential relaxation in molecular and electronic glasses, *Rep. Prog. Phys.*, **59** (1996), 1133. http://dx.doi.org/10.1088/0034-4885/59/9/003

28. H. H. Ahmad, M. Aboshady, M. Mansour, The role of risk factors in system performance: a comprehensive study with adaptive progressive type-ii censoring, *Mathematics*, **12** (2024), 1763. http://dx.doi.org/10.3390/math12111763

29. C. P. Robert, G. Casella, *Monte Carlo statistical methods*, New York: Springer, 2004. http://dx.doi.org/10.1007/978-1-4757-4145-2

Appendix A. Algorithm for T80 Prediction

```
1. Load Time and Efficiency from DATA.xlsx
2. A_guess = Efficiency(1); E_norm = Efficiency / A_guess
3. Linearize: y = log(-log(E_norm)), x = log(Time) for 0<E_norm<1
4. p = polyfit(x, y, 1); beta_guess = p(1); B_guess = exp(p(2)/beta_guess)
5. Fit: A*exp(-(B*t)^beta) with start [A_guess, B_guess, beta_guess]
6. t80 = (1/B)*(-log(0.2*A_guess/A))^(1/beta)  // hours
7. Convert: t80 = round(((t80/24) - 5.5)*24, 2)  // hours after 5.5 days
```

Appendix B. Monte Carlo simulation for PHC model under adaptive censoring

```
Input:
    true_params = ($\alpha=0.8, \beta=1.5, \gamma=1.2$)
    n = sample size (25, 60, or 100)
    m = target failures (10, 20, or 35)
    T = ideal cutoff time (0.5 or 1.0)
    R = pre-fixed removal plan
    N_rep = 1000 (number of Monte Carlo repetitions)

Output:
    Bias, MSE, and coverage for each estimator

For rep = 1 to N_rep:
 1. Generate random sample of size n from PHC($\alpha,\beta,\gamma$)
    using inverse transform sampling
```

2. Apply adaptive progressive Type–II censoring (Section 4.1) to obtain censored data
3. Compute MLEs via fmincon (Section 5.1)
4. Compute Bayesian estimates via MCMC (Section 5.2)
5. Store estimates and compute reliability functions

End For

Compute performance metrics: Bias, MSE, 95% coverage probabilities

AIMS Press